frontiers | Frontiers in Cell and Developmental Biology

TYPE Original Research
PUBLISHED 20 November 2024
DOI 10.3389/fcell.2024.1481881

OPEN ACCESS

EDITED BY
Wei Guo,
Chinese Academy of Sciences (CAS), China

REVIEWED BY
Yang Li,
University of Michigan, United States
Jing He,
Institute of Zoology (CAS), China

*CORRESPONDENCE
Attilio Pane,
apane@icb.ufrj.br

RECEIVED 10 September 2024
ACCEPTED 05 November 2024
PUBLISHED 20 November 2024

CITATION
Brito TFd, Arruda Cardoso M, Atinbayeva N, Alexandre de Abreu Brito I, Amaro da Costa L, Iovino N and Pane A (2024) Embryonic piRNAs target horizontally transferred vertebrate transposons in assassin bugs.
Front. Cell Dev. Biol. 12:1481881.
doi: 10.3389/fcell.2024.1481881

Embryonic piRNAs target horizontally transferred vertebrate transposons in assassin bugs

Tarcísio Fontenele de Brito[1], Maira Arruda Cardoso[1], Nazerke Atinbayeva[2,3], Ingrid Alexandre de Abreu Brito[1], Lucas Amaro da Costa[1], Nicola Iovino[2] and Attilio Pane[1,4]*

[1]Instituto de Ciências Biomédicas, Universidade Federal do Rio de Janeiro, Rio de Janeiro, Brazil, [2]Department of Chromatin Regulation, Max Planck Institute of Immunobiology and Epigenetics, Freiburg im Breisgau, Germany, [3]Albert-Ludwigs-Universität Freiburg, Freiburg im Breisgau, Germany, [4]Instituto Nacional de Ciência e Tecnologia em Entomologia Molecular, Rio de Janeiro, Brazil

Introduction: Piwi proteins and the associated Piwi-interacting RNAs (piRNAs) coordinate a surveillance system that protects the animal genome from DNA damage induced by transposable element (TE) mobilization. While the pathway has been described in detail in the fruit fly *Drosophila melanogaster*, much less is known in more basal insects. *Rhodnius prolixus* is an hemipteran insect and one of the major vectors of Chagas disease. *Rhodnius* acquired specific classes of horizontally transferred transposons (HTTs) by feeding on bats, opossums and squirrel monkeys, thus providing the opportunity to investigate the piRNA-base response against HTTs in this species.

Methods: SmallRNA-Seq reads mapping to HTTs and resident transposable elements were quantified and checked for piRNA features like 1U a 10A biases, ping-pong and phasing signatures. Uniquely mapped piRNAs were used to identify piRNA clusters in *Rhodnius*' genome. RNA-Seq data was used to quantify transposon and Rp-PIWI genes expression levels and were validated by qRT-PCR.

Results: By analyzing the temporal dynamics of piRNA cluster expression and piRNA production during critical stages of Rhodnius development, we show that peak levels of ~28 nt long piRNAs correlate with reduced HTT and resident TE expression primarily during embryogenesis. Strikingly, while resident TEs piRNAs seem to engage in a typical ping-pong amplification mechanism, sense and antisense HTT piRNAs instead overlap by ~20 nt or do not display ping-pong signatures.

Discussion: Our data shed light on the biogenesis and functions of the piRNAs in Rhodnius prolixus and reveal that piRNAs, but not the siRNA pathway, responded to HTTs that were recently transferred from vertebrate tetrapods to a hematophagous insect of medical relevance.

KEYWORDS

rhodnius, HTT, piRNA pathway, transposon, siRNA

Introduction

Transposable elements (TEs) are selfish genetic elements that can mobilize and insert in new positions of eukaryotic genomes. These sequences often comprise a substantial proportion of the host genome reaching more than half of the human genome and 90% of the maize genome (SanMiguel et al., 1996; Lander et al., 2001; Hubley et al., 2016). Although TEs are usually passed on to the next generations via vertical transmission, a growing body of evidence is showing that horizontal transposons transfer (HTT) is more widespread than previously appreciated and occurs not only between closely related species, but also across distant phyla (Kofler et al., 2015; Peccoud et al., 2017; Zhang et al., 2020). One of the most remarkable examples is represented by the horizontal transfer of DNA transposons between the triatomine insect *Rhodnius prolixus* and vertebrates, which occurred within the past 50 millions years (Gilbert et al., 2010). *Rhodnius* is a hematophagous insect species and a primary vector of *Trypanosoma cruzi*, the causative agent of Chagas disease. Transposons of the *SPACE INVADERS* (*SPIN*), *OposCharlie1* (*OC1*), *hAT1* and *ExtraTerrestrial* (*ET*) in the genome of this insect were found to share up to ~98.1% sequence identity with those described in opossums, squirrel monkeys and bats of South America (Gilbert et al., 2010). *Rhodnius* likely acquired the HTTs from these vertebrates because of its blood-feeding habit and the broad range of hosts. The same habit is responsible for the transmission of *T. cruzi* to humans and underlies the etiology of Chagas disease. *Rhodnius* also harbors other promiscuous transposons like *RTE-X*, *Ty3 retrotransposon, Helitron, I, Maverick* and *Mariner*, with the latter being the predominant family in the *Rhodnius* genome (Filée et al., 2015). These TEs are often transmitted horizontally across the animal kingdom and even between animals and plants (Gao et al., 2017). How cells respond to newly invading transposons has been investigated in the fruit fly *D. melanogaster*. The best characterized example of HTT involves the horizontal transfer of P-elements from *Drosophila willistoni* to *D. melanogaster* and their subsequent spreading across natural *Drosophila melanogaster* populations over the second half of the 20th century (Kidwell et al., 1988). P-element invasion of a naive genome was soon associated with a class of developmental defects collectively known as hybrid dysgenesis (Kidwell et al., 1977; Daniels et al., 1990). Hybrid dysgenesis leads to sterility but only manifests itself in the progeny that paternally inherits the P-element. The discovery of the piRNA pathway and its crucial role as a defense system against transposon-induced DNA damage allowed to shed light on the molecular underpinnings of hybrid dysgenesis (Brennecke et al., 2008). Piwi-interacting RNAs or piRNAs are a class of small non-coding RNAs ranging in size from 18 to 30 nucleotides that are typically found in complex with PIWI proteins (Cox et al., 2000; Yin and Lin, 2007; Czech et al., 2018). The pathway has been best described in *D. melanogaster* and a few other holometabolous insect species (Santos et al., 2023). In *Drosophila* somatic cells, piRNA precursor transcripts originate from regions of the genome harboring a variety of transposon remnants known as piRNA clusters (Brennecke et al., 2007; Gunawardane et al., 2007). These piRNA precursors are processed in cytoplasmic organelles known as Yb-bodies to generate mature mostly antisense piRNAs (Saito et al., 2010). In turn, antisense piRNAs are loaded into the Piwi protein that translocates to the nucleus and employs them as guides to identify and silence actively transcribed transposons in the genome (Sienski et al., 2012; Le Thomas et al., 2013). Among the primary targets of the somatic pathway are the *Zam*, *Ty3 retrotransposon* and *Idefix* transposons (Pélisson et al., 1994; Brennecke et al., 2007; Zanni et al., 2013). The transcription of the germline piRNA clusters instead occurs from both genomic strands (i.e., dual-strand piRNA clusters) (Brennecke et al., 2007) and is regulated by a dedicated machinery (Klattenhoff et al., 2009; Pane et al., 2011; Mohn et al., 2014; Andersen et al., 2017). Cluster transcripts produce primary antisense piRNAs as in the somatic cells (Malone et al., 2009). However, a fraction of these RNAs promotes a feedforward amplification loop known as the "ping-pong" cycle, that is regulated by Aubergine (Aub) and Argonaute3 (Ago3) (Brennecke et al., 2007; Gunawardane et al., 2007). The loop starts when Aub bound to primary antisense piRNAs elicits the formation of sense piRNAs by cleaving the transcripts of active transposons. In turn, sense piRNAs are bound by Ago3, which can now recognize cluster transcripts to produce more antisense piRNAs. The slicing activities of Aub and Ago3 leave a typical hallmark in the secondary piRNA complement known as "ping-pong signature", whereby sense and antisense piRNAs overlap by 10 nt at their 5′end. Also, because antisense piRNAs display a 5′Uracil bias (1U), the sense piRNA mates are enriched with an Adenine residue at the 10th position (10A). Antisense piRNAs associate with Piwi also in the germline and guide the protein to the nucleus.The ping-pong cycle is also involved in the production of phased primary piRNAs (Han et al., 2015). Once a piRNA precursor is cleaved by Ago3 or Aub to generate a secondary piRNA, the remaining sequence immediately after the 3′ end of the cleavage site is successively clipped and trimmed. The mechanism is widely conserved among animal species, increasing not only the number but also the diversity of piRNA sequences (Han et al., 2015; Gainetdinov et al., 2018). In addition to the piRNA pathway, endogenous ~22 nt long siRNAs (siRNAs) have also been implicated in transposon downregulation in *Drosophila* (Czech et al., 2008; Rosenkranz et al., 2015). siRNAs are generated through the cleavage double-strand RNA molecules by the ribonuclease Dicer2 (Dcr2) and loaded into Argonaute2 (Ago2) to form the RISC complex (Bernstein et al., 2001; Lee et al., 2004). Transposon-related siRNAs can originate from piRNA clusters or from transposable elements (Czech et al., 2008). In *Drosophila*, the siRNA pathway downregulates certain TEs in the somatic cells, while the piRNA pathway is crucial in germline tissues.

Since the discovery of horizontally transmitted P-elements in *Drosophila* species, a wealth of studies have reported the exchange of transposable elements between non-hybridizing insect species (Daniels et al., 1990; Peccoud et al., 2017; Carvalho et al., 2023). The piRNA pathway has been proposed to coordinate an adaptive defense mechanism against newly invading transposons (Aravin et al., 2007). A naive genome would not express piRNAs against a new TE, which can therefore insert in several positions in the genome. However, when a transposon copy eventually integrates in a piRNA cluster, it becomes a source of piRNAs that guide the PIWIs to silence in *trans* the active elements dispersed in the genome. The observation that piRNAs are maternally loaded in the developing eggs also pointed out a mechanism to explain the hybrid dysgenesis syndrome (Brennecke et al., 2008). The progeny of a cross between a female fly bearing a P-element and a naive male will

10.3389/fcell.2024.1481881

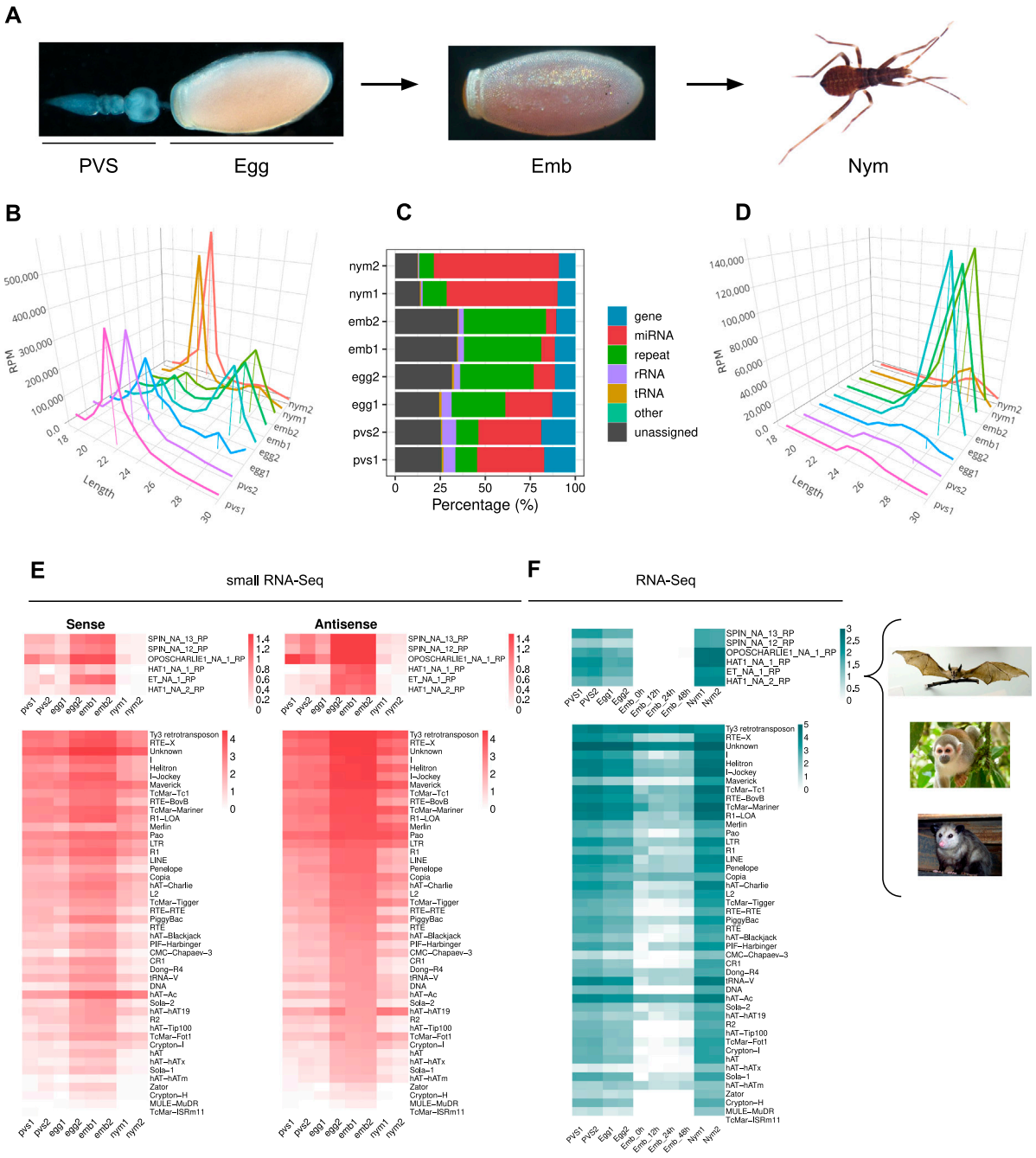

FIGURE 1
Rhodnius prolixus embryos express ~28 nt long piRNAs targeting Horizontally Transferred Transposons (HTT) and resident TEs. **(A)** Developmental stages of *Rhodnius prolixus* analyzed in the current study. For oogenesis, we investigate the previtellogenic stage (PVS) comprising the tropharium and early follicles independently of the mature chorionated eggs dissected from the female abdomen (Egg). Embryos (Emb) were collected over a 48 h period encompassing the cleavage stage until the formation of the head and thoracic segments after gastrulation. First instar nymphs (Nym) were also analyzed to investigate postembryonic development. **(B)** Length distribution of all mapped reads for each replicate displayed in RPM. The ~22 nt and ~28 nt peaks were anchored to the *X*-axis (Length) for a better visualization. *Y*-axis displays RPM values. For each sample, we produced two replicates, which were analyzed separately. **(C)** Small RNA profiling based on percentage of reads mapped to annotated and unannotated (unassigned) regions of *Rhodnius* genome. miRNAs are particularly abundant in oogenesis and postembryonic development (red), while embryonic stages are dominated by repeat-associated small RNAs (green). **(D)** Length distribution of reads mapped to transposable and repetitive sequences of *Rhodnius* displayed in RPM. A major peak comprising ~28 nt piRNAs is clearly detectable in the two embryo replicates (Emb1 and Emb2) and in one of the mature egg replicates (Egg2). This class of small non-coding RNAs is less abundant in previtellogenic stages of oogenesis (PVS1 and PVS2 replicates), in one of the mature egg replicates (Egg1) and in 1st instar nymphs (Nym1 and Nym2 replicates). **(E)** Heatmaps displaying the expression levels of sense and antisense piRNAs for each TE subfamily in PVS, Egg, Emb and Nym stages. Sense and antisense piRNAs for the horizontally transmitted transposons (HTT) ET, SPIN, OC1 and hAT and for the resident TEs are shown separately. Colorbar values display $\log_{10}$(RPM +1). **(F)** Heatmaps showing TE expression levels as per RNA-Seq in PVS, Egg, Emb and Nym stages. Expression levels for the HTTs ET, SPIN, OC1 and hAT and of the resident TEs are displayed in separate heatmaps. Colorbar values display RPKM. *Rhodnius* acquired the HTTs from opossums, squirrel monkeys and bats (right). For the SPIN and hAT families, Gilbert and coworkers reported two transposon sequences for SPIN and hAT, namely, SPIN_NA_13_RP, SPIN_NA_12_RP, hAT_NA_1_RP and hAT_NA_2_RP. One transposon

(*Continued*)

FIGURE 1 (Continued)
sequence was reported for ET and OC1, which were labeled ET_NA_1_RP and OPSCHARLIE1_NA_1_RP, respectively. For simplicity, we refer to these transposable elements as SPIN, hAT, OC1 and ET throughout the article. Images of bat, squirrel monkey and opossum with Public Domain license were obtained from Wikimedia Commons.

develop normally because it inherits both the TE and the cognate piRNA set. In contrast, the reciprocal cross will prove sterile because the P-element is transmitted by the father to a progeny that lacks the appropriate piRNA set. Aside from the Drosophilids however, much less is known about the mechanisms that allow insect species to repress newly invading transposons. The piRNA pathway is evolutionarily conserved in animals, but remarkable differences can be observed even when the investigation is restricted to species of the same genus (Dowling et al., 2016; Chary and Hayashi, 2023; Santos et al., 2023). For instance, it was recently shown that *Drosophila eugracilis*, which diverged only 10 million years ago from *D. melanogaster*, neither uses a ping-pong amplification mechanism nor it expresses the critical YB protein (Chary and Hayashi, 2023). The expression patterns and size distribution of the piRNAs also varies when *D. melanogaster* is compared to other holometabolous insects like *Tribolium casteneum*, *Bombyx mori* and *Apis mellifera* (Aravin et al., 2001; Ninova et al., 2017; Wang et al., 2017; Llonga et al., 2018). In hemimetabolous insects the characterization of the pathway is still in its infancy, but it was shown that *Blattella germanica* expresses ~28 nt piRNAs during embryogenesis as well as stage-specific piRNA pools during post embryonic development (Llonga et al., 2018). Remarkably, while the most conserved function of the piRNA pathway is connected to transposon silencing and genome stability, the PIWI proteins have been shown to coordinate antiviral mechanisms in mosquitos, sex determination in silkworms and maternal RNA degradation in various insect species (Santos et al., 2023). Thus, the investigation of the piRNA pathway in more basal insects might reveal novel mechanisms and functions and shed light on the arms race between transposons and related defense systems.

Rhodnius prolixus is a hemimetabolous insect belonging to the Triatomine subfamily and undergoes 5 nymph stages during development before turning into a fertile winged adult (Buxton, 1930). Blood feeding is not only necessary for ecdysis, but also to trigger oogenesis in adult females. Because of these features, *Rhodnius* has been extensively studied to dissect insect physiology and metabolism over the past century. Despite the sequencing and partial assembly of the genome however, the genetic and molecular mechanisms driving its development are lagging behind. The repertoire of miRNAs has only started to be unraveled, while the structure and function of piRNAs in this insect species are completely unknown. It was estimated that between 19% and 23% of the *Rhodnius* genome is composed of transposon sequences with the *Mariner* family accounting for a large fraction of the mobilome (Filée et al., 2015; Mesquita et al., 2015; Montiel et al., 2021). The genome of this hemipteran insect harbors four *PIWI* genes and we have previously shown that *Rp-piwi2*, *Rp-piwi3* and *Rp-ago3*, but not *Rp-piwi1*, are expressed in ovaries and are necessary for female adult fertility (Brito et al., 2018). Furthermore, our transcriptomic analyses revealed that orthologs of the *Drosophila* piRNA and siRNA pathways components are also expressed in *Rhodnius* ovaries (Coelho et al., 2021). In this study, we characterize the temporal dynamics of the piRNAs and their source *loci* in the *Rhodnius* genome. Importantly, we provide the first evidence of the ability of the piRNA pathway to respond and adapt to HTTs transmitted from vertebrates to a hematophagous insect responsible for the transmission of Chagas disease.

Results

Small RNA profiling in *Rhodnius prolixus*

In order to investigate the dynamics of piRNA expression in oogenesis and early stages of *Rhodnius* development, we generated and sequenced small RNA libraries from embryos (Emb) and 1st instar nymphs (Nym) and analyzed them together with small RNA datasets from previtellogenic stages of oogenesis (PVS) and mature eggs (Egg), that we previously produced (Brito et al., 2021) (Figure 1A). After trimming and quality checking, we mapped the reads to the RproC3 version of *Rhodnius* genome available at VectorBase (Giraldo-Calderón et al., 2015; Mesquita et al., 2015). The percentage of reads that mapped to the genome ranged from ~86% for the PVS1 replicate to ~95% for the Egg2 replicate (Supplementary Table S1). The length distribution of the reads reveals a bimodal distribution with two major peaks at ~22 nt and ~28 nt (Figure 1B). The former is more prominent in PVS, Egg1 and Nym samples, while the latter is more apparent in Egg2 and Emb samples. To gain insight into the complexity of *Rhodnius* small RNAs, we contrasted our small RNA datasets against *Rhodnius* annotated features available at VectorBase (Giraldo-Calderón et al., 2015). As expected, a substantial proportion of the mapped reads (i.e. 36.16% for PVS and 65.52% for Nym), match annotated miRNAs (Figure 1C). The abundance of reads corresponding to repetitive sequences shows a reciprocal distribution when compared to the miRNAs. In fact, this category is highly expressed in embryos, while it's progressively lower in PVS (12.07%) and Nym (10.6%). Once again, the Egg replicates display two non-overlapping distributions with Egg2 being more comparable to the Emb replicates. Other genomic features, including tRNAs, are below 8% in all the samples. A fraction of the reads, ranging from ~12% in Nym to ~34% in Emb, could not be classified based on annotated features (i.e., "unassigned"). Next, we profiled the length distribution of the reads associated with transposons and repetitive sequences (Figure 1D). All the stages analyzed displayed an apparent peak at 21–22 nt, that likely comprises siRNAs, and a ~28 nt peak corresponding to piRNAs. The abundance of these classes of small RNAs varies in the different samples. The ~22 nt population is predominant in PVS, while the ~28 nt is dramatically expressed in embryonic stages and largely exceeds the ~22 nt set (Figure 1D). In nymph stages, the levels of ~22 nt and ~28 nt small RNAs seem comparable. Once again, the Egg1 and

10.3389/fcell.2024.1481881

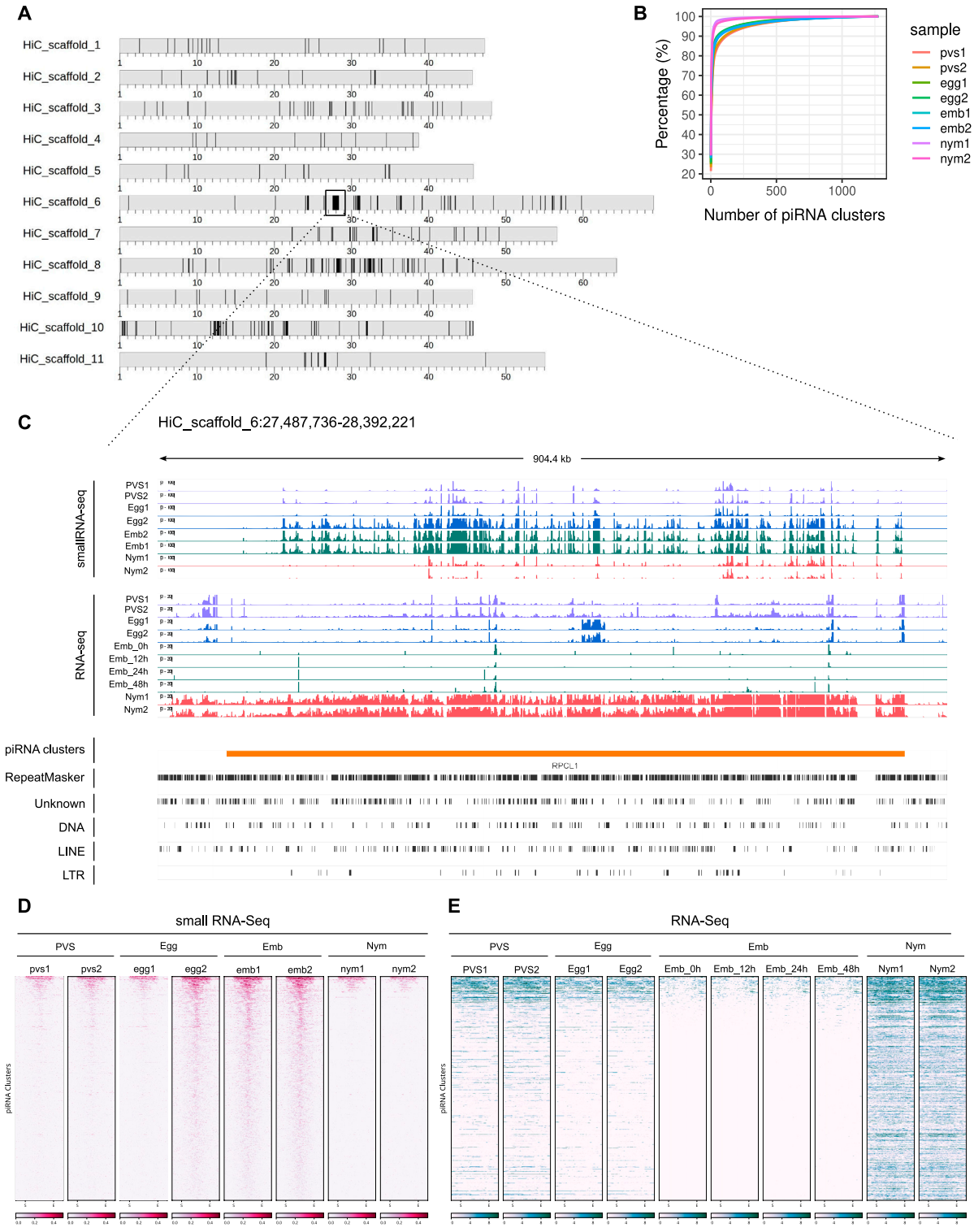

FIGURE 2
piRNA clusters are a major source of piRNAs during *Rhodnius prolixus* embryonic development. **(A)** Ideograms of the larger scaffolds obtained from the HiC genome assembly that likely represent the 10 autosomes and the X chromosome (scaffold 10) of *Rhodnius*. Each ideogram is scaled to the size of each scaffold, with a scale in megabases. Black vertical lines show the distribution of the piRNA clusters. The major cluster RPCL1 is highlighted (black box). **(B)** Cumulative percentage of piRNAs in clusters for each replicate. The top 10 RPCLs account for 74% of the total uniquely mapping piRNAs. **(C)** IGV (Robinson et al., 2011) visualization of the RPCL1 cluster region on the HiC_scaffold_6. Uniquely mapped piRNAs for each stage are profiled for each sample (small RNA-Seq profiles). The *Y*-axis displays RPM (0–100 interval). Expression levels of the RPCL1 (RNA-Seq) in all the stages are also displayed. Of note, we included in this analysis the RNA-Seq datasets for embryonic stages 0, 12, 24 and 48 h post egg laying produced by Pacual and coworkers. The *Y*-axis displays the RPKM range 0–20. Orange bar highlights the position of the RPCL1 cluster. The distribution of DNA and LTR transposons together with LINE elements and unknown sequences along the RPCL1 region are reported with black boxes. **(D)** Heatmaps showing the temporal regulation of the cluster-derived mature piRNAs (Small RNA-seq) and piRNA precursor transcripts (RNA-Seq) in PVS, Egg, Emb and Nym stages. Mature piRNA levels

(*Continued*)

FIGURE 2 (Continued)
inversely correlate with the expression levels of cluster transcripts suggesting that piRNA biogenesis consumes cluster-derived transcripts during embryonic stages. Small RNA-seq values (left side of the panel) are displayed as $\log_{10}$(RPM +1), while RNA-Seq values (right side of the panel) are expressed as RPM. Each line of the heatmap represents a piRNA cluster with the major clusters at the top of the panels.

Egg2 replicates provided two different size distributions. Only Egg1 is compatible with maternally loaded piRNAs generated in PVS, while the second replicate seems more similar to the profile obtained in embryos. The easiest explanation for this observation is that the eggs dissected from the adult females used for the Egg2 replicate included a proportion of developing embryos that were retained by the mother. We decided to keep these replicates as they might help shed light on the very initial stages of embryogenesis.

It was shown that four DNA transposon families in *Rhodnius*, that is *SPIN, OC1, hAT* and *ET* originated by horizontal transfer from vertebrate tetrapods (Gilbert et al., 2010). We therefore wondered whether piRNAs related to these HTTs are expressed in *Rhodnius*. To answer this question, we attempted to isolate all the RNAs with 18–30 nt matching HTTs sequences. Strikingly, we find both sense and antisense piRNAs for 6 HTTs reported by Guilbert and collaborators (Figure 1E) (Gilbert et al., 2010). In addition to the HTTs, 46 transposon families produce both sense and antisense piRNAs with 14 families accounting for more than 90% of the piRNAs. Among them, we could detect abundant piRNAs *LTR/Ty3 retrotransposon*, the LINE elements *Jockey* and *RTE-X*, the rolling-circle *Helitron* and, as expected, for DNA transposons of the *Mariner* family (Figure 1E). The latter explains 8.9% of the total piRNAs. Among the top most piRNA-producing sequences, we find a class of "Unknown" elements, which might comprise novel transposons or repetitive sequences. In agreement with the general dynamics of the piRNA population in the different stages analyzed, the expression of both sense and antisense piRNAs for the HTTs and other resident TEs appears to dramatically increase during embryogenesis, with the antisense population being more prominent (Figures 1D, E).

We then analyzed the expression patterns of TEs in oogenesis and early *Rhdonius* development (Figure 1F). To this aim we combined ovarian and embryonic RNA-Seq datasets that we and others previously generated together with newly sequenced transcriptomes of 1st instar nymphs (Coelho et al., 2021; Pascual and Rivera-Pomar, 2022). The temporal expression dynamics of the TEs appear to inversely correlate with piRNA abundance in each stage. The highest TEs expression levels are observed in nymphs, while the lowest are detected in embryonic stages concomitant with peak levels of piRNAs. These results suggest that the 28 nt piRNA population might drive TE silencing during *Rhodnius* embryogenesis, while TE mobilization might be more tolerated in postembryonic development.

piRNAs in *Rhodnius prolixus* are produced from uni-strand clusters

In order to identify the piRNA source *loci* in *Rhodnius*, we narrowed down our search to piRNAs that map uniquely to the genome (Brennecke et al., 2007). For this study, we adopted a new version of the *Rhodnius* genome generated with the Hi-C technique and available at (https://www.dnazoo.org/assemblies/Rhodnius_prolixus). The Hi-C genome comprises 11 major scaffolds that likely represent the X chromosome and the 10 autosomes of *Rhodnius*. Scaffold 10 was proposed to actually correspond to the X chromosome. We found that unique piRNAs clusterize at 1,276 different positions in the genome mainly along the major scaffolds 1–11 (1,176) (Figure 2A). The top 10 clusters account for ~74% of the total unique piRNAs expressed in *Rhodnius* embryogenesis (Figure 2B). Only 16 RPCLs (i.e., *Rhodnius prolixus* clusters) display RPM >100 and 6 of them display RPM >1,000. These RPCL are hosted on scaffold 6 (RPCL1, RPCL3 and RPCL4), scaffold 11 (RPCL2) and the putative X chromosome scaffold 10 (RPCL5 and RPCL6). We find that transposons of the *LINE RTE-X*, *Jockey* and *Ty3 retrotransposon* families together with *Mariner*-like DNA transposons are the most abundant in the top 10 piRNA clusters (Supplementary Figure S1). It is worth noting however that the most abundant sequence belongs to the "unknown" category and deserves further investigation in the future. The clusters vary in size from a few kilobases to over 700 kb for the RPCL1 locus (Figure 2C). For the major RPCL1 cluster, we can observe a clear anticorrelation between the levels of piRNAs and cluster transcripts (Figure 2C). High piRNA levels in embryos coincide with low levels of cluster transcripts. Instead, cluster transcripts appear to accumulate in PVS and, especially, in nymphs, where piRNA expression is at the lowest. Similar expression patterns are observed for the majority of the piRNA clusters (Figures 2D, E).

Next, we investigated the expression of the cluster-derived piRNAs in PVS, Egg, Emb and Nym stages (Figure 3). Once again, we took into account only uniquely mapping piRNAs. Consistent with the general piRNA temporal profile, the top 10 piRNA clusters display a stark increase in the expression of piRNAs during embryonic stages (Figures 3A, B). Importantly, these *loci* give rise to sense and antisense piRNA populations with the latter generally being more abundant (Figures 3A, B). The alignment of the unique mappers demonstrates that the majority of the clusters are of the uni-strand type (Figure 3C). Among the major clusters, we were unable to unambiguously identify dual-strand or bidirectional *loci* in *Rhodnius*. RPCL2, which spans over 200 kb, initially appeared to be a bidirectional *locus* in that part of the cluster seems to be expressed from (+) strand and the other from the (−) strand of the genome (Supplementary Figure S2). Yet, upon closer inspection we realized that the region between the two parts of the cluster with opposite profiles was only partially sequenced. Thus, RPCL2, like other instances of seemingly bidirectional clusters, might represent a genome assembly error, but a more precise characterization will require an improved assembly of the *Rhodnius* genome. We then looked at the orientation of the transposons within the top 20 piRNA clusters (Figure 3D). Different from the *D. melanogaster flam* locus, where transposon fragments are polarized, *Rhodnius* clusters harbor transposons on both genomic strands. Thus, these *loci* can produce both sense and antisense piRNA, even though transcription occurs from one strand of the genome.

Because Rhodnius embryos produce piRNAs targeting the HTTs, we wondered whether these transposons or their

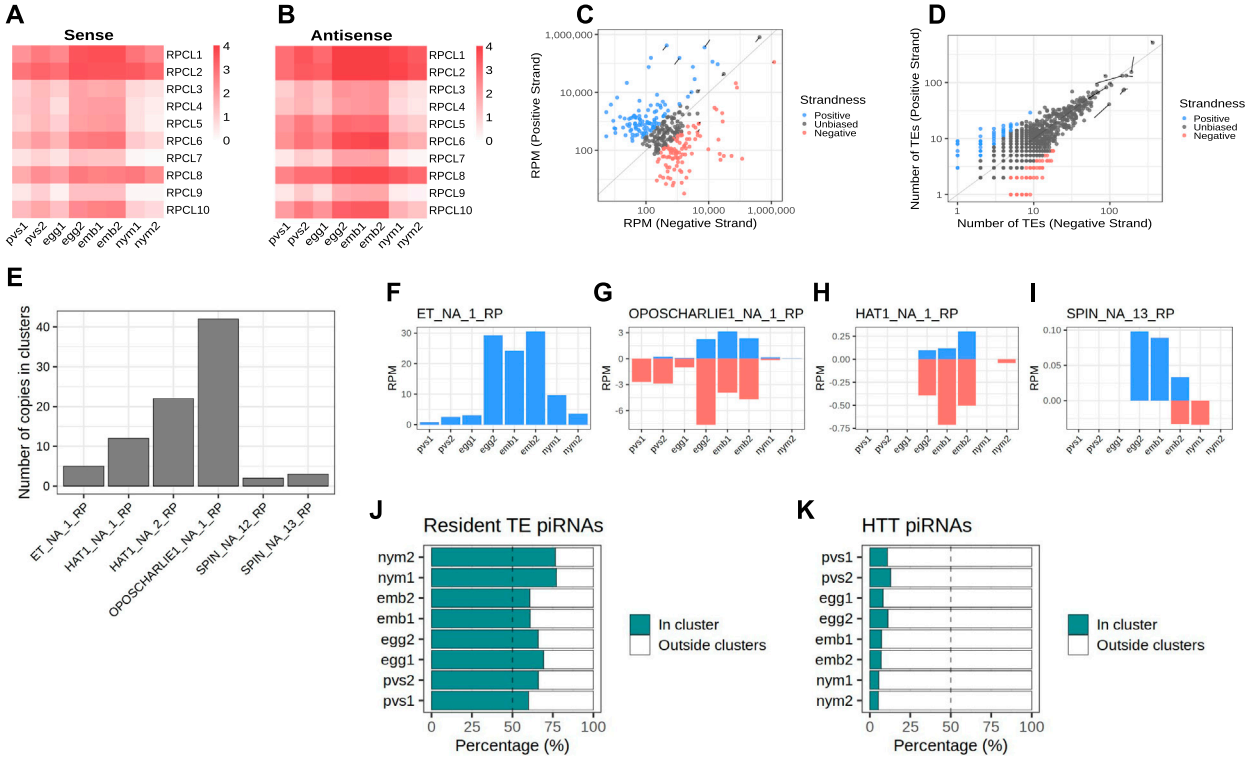

FIGURE 3
Rhodnius piRNA clusters are uni-strand and produce piRNAs against HTTs. **(A, B)** Heatmaps showing sense **(A)** and antisense **(B)** piRNA levels for the top 10 piRNA clusters in PVS, Egg, Emb and Nym stages. Colorbar displays log_{10}(RPM +1). **(C)** Scatterplot reporting the strandness of the piRNA clusters. piRNA clusters primarily expressed from the +strand (blue dots) and -strand (red dots) of the genome are displayed. piRNA clusters with apparently unbiased expression are indicated (dark grey dots). A cluster was considered unbiased if less than 75% of its piRNAs could be attributed to a specific strand of the genome. *Y*-axis values are expressed as RPM. The top 10 piRNA clusters are highlighted. **(D)** Scatterplot showing the orientation of the TE fragment within each piRNA cluster. piRNA clusters harboring TEs predominantly on the +strand (blue dots) or -strand (red dots) of the genome are reported. These categories are mostly formed by small clusters with a low number of TEs. The vast majority of the piRNA clusters are characterized by unbiased distribution of TEs (dark grey dots). The top 10 piRNA clusters are highlighted. **(E)** Number of HTT copies inserted into the piRNA clusters. **(F–I)** piRNAs uniquely mapping to the cluster HTTs. The ET copies **(F)** seem to exclusively produce sense piRNAs, while OC1 **(G)**, hAT **(H)** and SPIN **(I)** generate both sense and antisense piRNAs. *Y*-axis displays RPM values. *X*-axis shows the replicates for the PVS, Egg, Emb and Nym samples. **(J)** Percentage of uniquely mapping piRNAs for the resident TEs originating from within or outside the piRNA clusters. **(K)** Percentage of uniquely mapping piRNAs for the HTTs originating from within or outside the piRNA clusters.

fragments are inserted into the piRNA clusters. To answer this question, we aligned the *SPIN*, *hAT*, *OC1* and *ET* sequences with the *Rhodnius* HiC genome and counted the number of occurrences within the piRNA clusters. In agreement with a recent horizontal transfer from vertebrates, the number of HTT copies in the clusters is low and ranges from less than 5 for *ET* and *SPIN* to ~40 for *OC1* (Figure 3E). The observation that HTTs sequences are inserted in the major clusters albeit with very low copy numbers prompted us to ask whether these copies are expressed and produce piRNAs. We observe that the *SPIN*, *OC1* and *hAT* sequences generate both sense and antisense piRNAs, while the *ET* element seems to produce mostly sense piRNAs (Figures 3F–I). These piRNAs however represent only a fraction of the HTT piRNAs. When we compare the cluster-derived piRNAs for resident TEs and HTTs, we observe a striking difference. While for the resident TEs between ~60% and ~80% of the piRNAs originate from the clusters (Figure 3J), less than 15% of the HTT piRNAs are produced from these loci (Figure 3K). Thus HTT piRNAs are mostly generated by the transposon copies scattered in the genome.

HTT piRNAs display unique features

In order to investigate the characteristics of the HTT piRNAs, we first profiled the piRNAs along the transposon sequences. Their distribution is not homogenous and they seem to accumulate at certain positions (Figures 4A–D). We then investigated the overlap between the 5′ ends of sense and antisense sequences for the paired piRNAs (Figures 4A′–D′). The 10 nt overlap typical of the ping-pong mechanism is either modest or it is confused among other peaks, as in the cases of *OC1* and *ET* (Figures 4A′, 4B′). Instead, the *SPIN* and *hAT* piRNA mates display an apparent ~20 nt overlap (Figures 4C′, 4D′), that is characteristic of siRNA heteroduplexes produced by the activity of the Dcr2 enzyme. Yet, these piRNA pairs are over 28 nt long. We next investigated the nucleotide distribution frequencies along the HTT piRNAs. We find that both sense and antisense piRNAs display a 1U bias, while the 10A bias in sense piRNAs is less apparent (Figures 4A″–D″). The most abundant piRNA pairs for *hAT* and *Spin* further underscore the unique properties of the HTTs piRNAs (Figures 4C, D inset). These pairs comprise piRNAs of over 28 nt in length, which overlap by

10.3389/fcell.2024.1481881

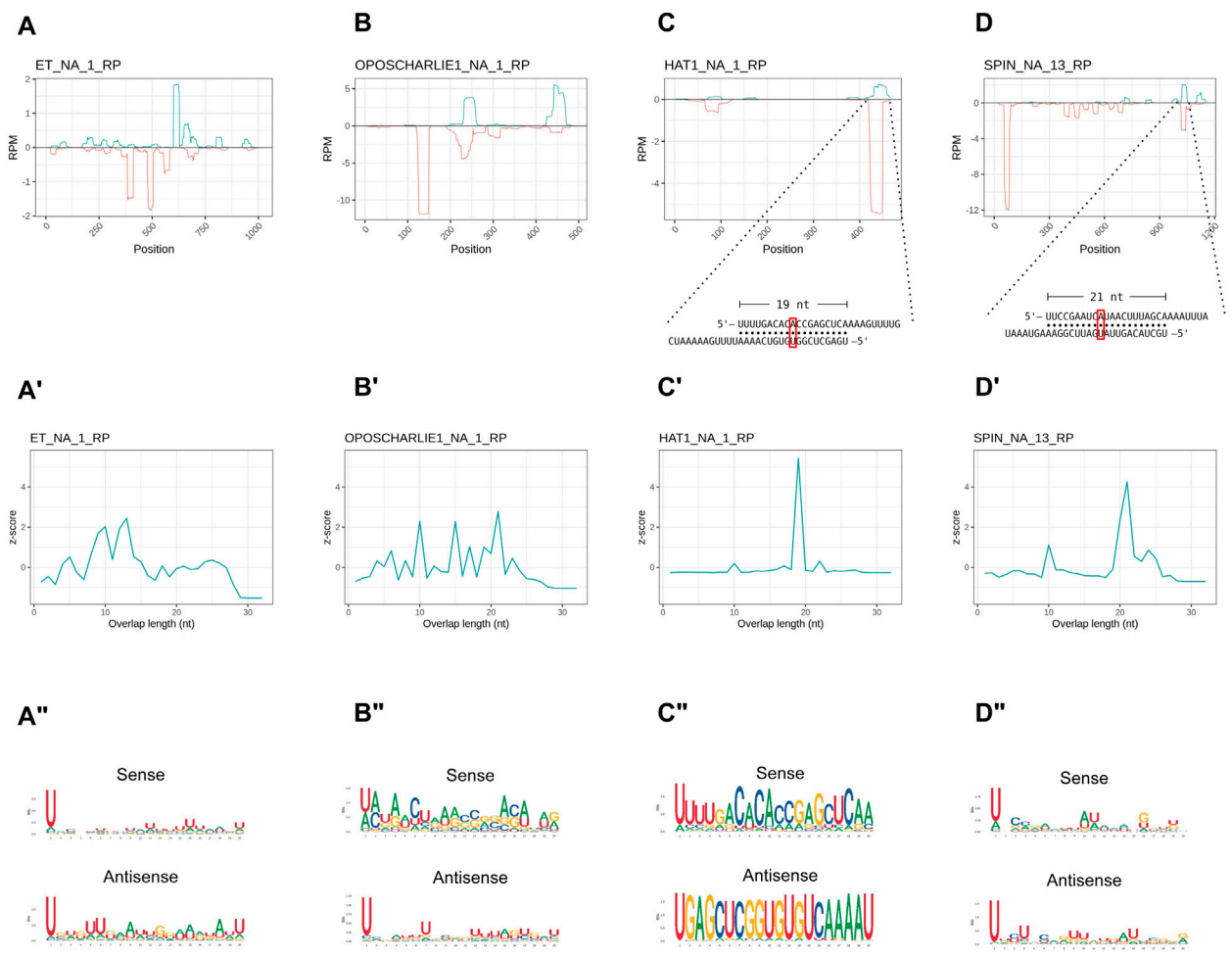

FIGURE 4
HTT piRNAs do not engage in a canonical ping-pong amplification mechanism. **(A–D)** piRNA profiling along the sequences of each HTT with sense piRNAs displayed with positive RPM values (green) and antisense piRNAs with negative RPM values (red). For the hAT and SPIN elements, the most abundant sense/antisense piRNA pairs are shown. Of note, the sense piRNAs pairs do not display the typical ping-pong signature, but overlap by ~20 nt. Yet, the sense mate for each pair bears an Adenine residue at the 10th position (red box). **(A′–D′)** 5′ to 5′ overlap length frequency reported as z-score values for each HTT. **(A′′–D′′)** Sequence logos displaying nucleotide bias for sense and antisense piRNAs mapped to the HTTs.

19 nt and 21 nt respectively. Remarkably both sense and antisense piRNAs display 1U and 10A residues for the *hAT* pair, while only the sense *Spin* piRNA has a 10A residue.

piRNAs in *Rhodnius prolixus* display ping-pong and phasing signatures

The HTTs have been suggested to have invaded the *Rhodnius* genome over the past 50 million years. Thus, the piRNAs associated with these elements likely display peculiar characteristics that are not shared by other resident TEs. To shed light on this aspect, we filtered all the small RNA sequences ranging from 24 to 30 nt in length, which yielded ~36 million putative piRNA sequences (Supplementary Table S2). We then investigated whether a ping-pong amplification system is active during *Rhodnius* development (Figure 5). First, we estimated the fraction of paired piRNAs in all the stages and found that it ranged from ~19% in PVS to ~29% in Embryos (Figure 5A). As expected the proportion of unpaired piRNAs is more abundant and likely comprises primary piRNAs. Different from the HTTs, we found that a substantial fraction of the pairs (~37%) overlap by exactly 10 nt at their 5′ends (Figure 5B). The analysis of nucleotide distribution shows that antisense piRNAs display a clear 1U bias in all the samples and that sense piRNAs are enriched with a 10A residue (Figure 5C). Sense piRNAs also bear a 1U bias, which was also described in *Tribolium castaneum*, although its meaning remains unclear. Thus, piRNAs engage in a ping-pong amplification mechanism in *Rhodnius*, which is not restricted to the germline as in *D. melanogaster*, but is also active in embryos and 1st instar nymphs. Previous studies demonstrated that piRNA production via ping-pong cycle is coupled with production of phased primary piRNAs in a range of different animals (Han et al., 2015; Gainetdinov et al., 2018). To address whether primary piRNAs can be produced in a phased manner, we compared the distances between 3′ and 5′ ends of different piRNAs mapped to the genome (Figure 5D). We find that a high frequency of consecutive piRNAs ($Z_0 > 9$) can be detected in all the stages. Therefore, phased primary piRNAs are produced in

10.3389/fcell.2024.1481881

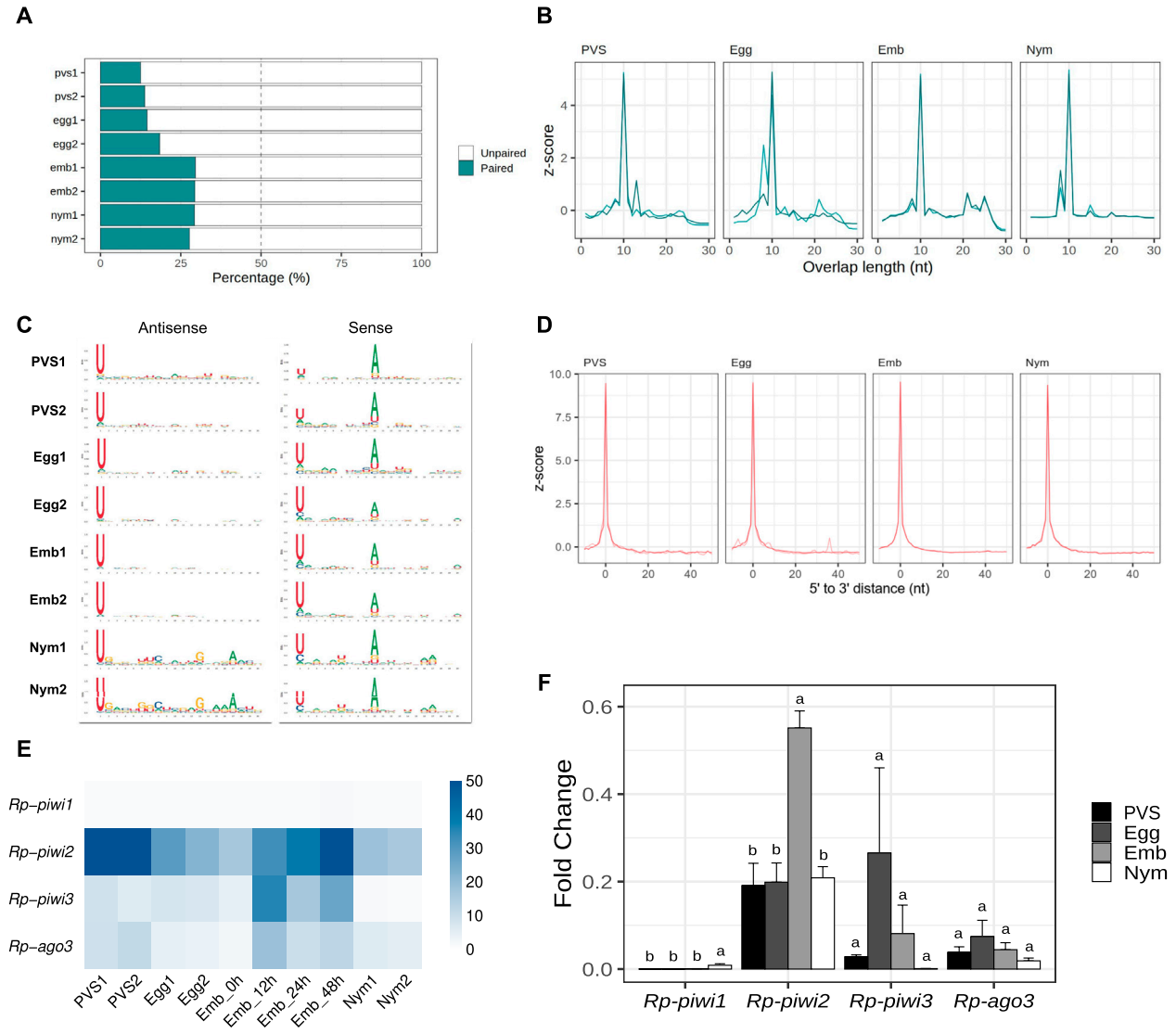

FIGURE 5
The ping-pong amplification loop is active in *Rhodnius prolixus*. **(A)** Percentage of paired and unpaired piRNAs for PVS, Egg, Emb and Nym replicates. **(B)** 5′ to 5′ overlap length frequency displayed in z-score for piRNAs mapped to resident transposons for each stage. **(C)** Sequence logo showing nucleotide bias for each position of antisense and sense piRNAs mapped to transposable elements in all the replicates. **(D)** Phasing quantification in z-score showing the 5′ to 3′ distance between consecutive piRNAs for each stage. **(E)** RNA-Seq analysis of the *Rp-PIWI* gene expression in oogenesis and early *Rhodnius* development. Colorcode displays RPKM values. **(F)** qRT-PCR analysis of the temporal expression levels of the *Rp-PIWI* genes during oogenesis and early stages of *Rhodnius prolixus* development. PVS = previtellogenic stage, Egg = mature chorionated eggs, Emb = embryos and Nym = 1st instar nymphs. *Y*-axis shows the mean Fold Change. Error bars display standard deviation from the mean. Statistical differences between stages were performed using one-way ANOVA followed by Turkey HSD *post hoc* test for pairwise comparisons ($p < 0.05$).

Rhodnius prolixus and likely share a similar mechanism of biogenesis as observed in other animals.

The discovery of a ~28 nt piRNA population in embryos and their involvement in a ping-pong amplification loop prompted us to investigate what *Rp-PIWI* genes are expressed in this stage as well as in first instar nymphs. We have previously shown that *Rp-piwi2*, *Rp-piwi3* and *Rp-ago3*, but not *Rp-piwi1* are expressed in and important for oogenesis in *Rhodnius* (Brito et al., 2018). In order to expand this analysis, we combined *in silico* and wet biology analyses (Figures 5E, F). First, we interrogated our RNA-Seq datasets together with those produced by Pascual and Rivera-Pomar (Pascual and Rivera-Pomar, 2022). Consistent with our previous studies, *Rp-piwi2*, *Rp-piwi3* and *Rp-ago3* are expressed in *Rhodnius* oogenesis (Figure 5E) (Brito et al., 2018). Interestingly, these genes are also upregulated in the first 48 h of embryonic development, while their levels drop substantially once the 1st instar nymphs hatch (Figure 5E). During postembryonic development, the levels of *Rp-piwi3* are below detectable levels. *Rp-piwi1* is apparently not expressed in any of the stages analyzed. In order to validate these observations, we performed qRT-PCR assays on total RNA extracted from PVS, Egg, Emb (0–48 h) and Nym stages. We used oligonucleotide pairs specific for each *Rp-PIWI* gene and for *Rp-rp49*, which served as internal control (Figure 5F) (Brito et al., 2018). The Fold Changes of each gene are in line with RPKM values. Interestingly, the *Rp-piwi2* levels

10.3389/fcell.2024.1481881

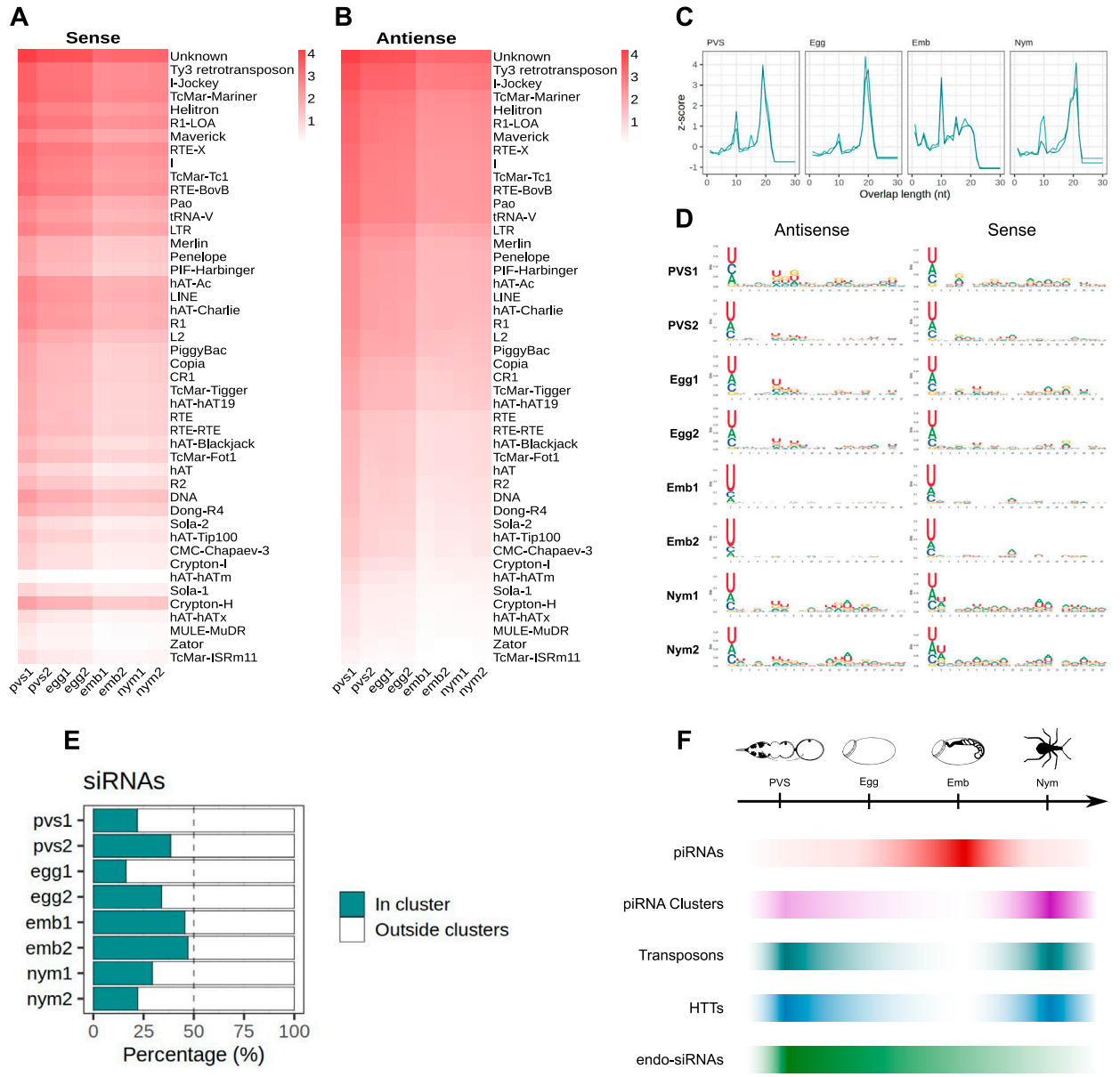

FIGURE 6
piRNA clusters generate ~22 nt siRNAs in *Rhodnius prolixus*. **(A, B)** Heatmaps showing sense **(A)** and antisense **(B)** ~22 nt long siRNAs mapped to the *Rhodnius* TE subfamilies. Colorbar displays $\log_{10}$(RPM +1). siRNAs appear to be expressed at higher levels in oogenesis compared to embryonic and postembryonic stages. **(C)** Z-scores of the 5′ to 5′ overlap length frequency for PVS, Egg, Emb and Nym samples. **(D)** Sequence logos showing nucleotide bias for each position of antisense and sense siRNAs for each stage. The 1U bias typical of the piRNAs is only detectable in embryos. **(E)** Percentage of uniquely mapping siRNAs originating from the piRNA clusters (green bars) versus other regions of the genome (white) for PVS, Egg, Emb and Nym stages. **(F)** Schematic diagram depicting the dynamics of piRNAs (red bar), piRNA cluster transcripts (purple bar), TEs (dark green), HTTs (blue bar) and siRNAs (light green bar) during oogenesis, embryogenesis and postembryonic development of *Rhodnius prolixus*.

dramatically increase in embryogenesis compared to the other stages analyzed and largely exceed those of the remaining *Rp-PIWIs* pointing to an important role in the biogenesis and/or function of the ~28 nt piRNA population. The expression of *Rp-piwi1* as per qRT-PCR is low, but clearly detectable and significantly different in 1st instar nymphs compared to other stages (Figure 5F). Whether *Rp-piwi1* transcripts exert any functions in postembryonic development remains to be elucidated. Our results reveal that *Rp-PIWI* genes are therefore temporally regulated during oogenesis and early *Rhodnius* development.

TE siRNAs are predominantly expressed in oogenesis

Although the piRNA pathway represents a major surveillance system keeping mobile elements in check, it was shown that Dcr2-dependent siRNAs control transposon silencing in *Drosophila* somatic cells (Kawamura et al., 2008). To investigate whether this mechanism is conserved in *Rhodnius*, we interrogated the transposon-related sequences in the 18 to 23 nt size range and analyzed the ping-pong signal, nucleotide bias and strandness

(Figure 6). We find a clear population of sense and antisense small RNAs centered on ~22 nt in length that is particularly abundant in PVS and Egg compared to the remaining samples (Figures 6A, B). Surprisingly, the two Egg replicates display remarkably similar siRNA profiles. Together with the piRNA analysis, this observation suggests that the Egg2 replicate might be capturing the early embryonic stages where the siRNA levels are still high, but the piRNA production from the zygotic genome is building up. The degree of overlap between sense and antisense sequences reveals that the ~22 nt small RNAs expressed in PVS, Egg and to a lesser extent in Emb and Nym are siRNAs, while Emb samples comprise ~22 nt piRNAs (Figure 6C). Consistent with this, the nucleotide distribution shows that the 1U together with a modest 10A bias are detected only in embryos, but not in the other stages analyzed (Figure 6D). Finally, we wondered whether TE siRNAs can originate from the piRNA clusters. The analysis of uniquely mapping reads reveals that a substantial proportion of siRNAs can indeed be produced by these *loci* in all the stages (Figure 6E). Accurate quantification of siRNAs produced from clusters versus TEs or other regions of the genome is confounded by the presence of piRNAs in the same size range. Surprisingly, we do not find sequences corresponding to the HTTs in the siRNA population. These observations reveal that siRNAs and piRNAs expression patterns are temporally regulated and partially overlap during oogenesis and early stages of *Rhodnius* development.

Discussion

Studies in *D. melanogaster* and its sibling species highlighted the adaptability of the piRNA pathway to newly invading transposons (Adaptation to P Element Transposon Invasion in Drosophila melanogaster, 2011). Aside from the Drosophilids however, how animal cells respond to TE invasion is still largely unknown. In this study, we show a striking example of piRNA pathway adaptation to TEs that were transferred from vertebrate tetrapods to the assassin bug *Rhodnius prolixus*. *Rhodnius* belongs to the Triatomine subfamily and has been firmly connected to the transmission of Chagas disease. It was shown that the *SPIN*, *OC1*, *hAT* and *ET* elements were horizontally transmitted to *Rhodnius* from bats, opossums and squirrel monkeys (Gilbert et al., 2010). Horizontal exchange of genetic material was already observed in the first version of *Rhodnius prolixus* genome, where 27 different genes have been exchanged between *Wolbachia* sp. and *Rhodnius* (Mesquita et al., 2015). These included transposases, one reverse transcriptase and recombination/repair enzymes, which might be involved in the Horizontal Gene Transfer (HGT) process. Recently, a systematic screen for HGT events conducted across 218 insect species shed light on the distribution of horizontally acquired genes across major groups (Li et al., 2022). The functions associated with the HGT-acquired genes varied greatly and the donors of the transferred genetic material are mainly bacteria, with a smaller portion deriving from fungi and plants (Li et al., 2022; Liu et al., 2023). Furthermore, it was revealed that the hemipteran insect *Bemisia tabaci* possesses the highest number of HGT genes among all insects. Interestingly, one of these genes is a plant-specific gene called *BtPMaT1*, which was acquired through feeding and helps the insect defend itself against toxins produced by plants (Xia et al., 2021). Because of the hematophagous habit of *Rhodnius* however, HTT might have occurred while the insect was feeding on the blood of the vertebrate hosts. This event provided the unique opportunity to investigate the response of the piRNA pathway to transposons exchanged between two different phyla in the past 50 million years. When we compare the complement of piRNAs targeting resident transposons and HTTs in *Rhodnius*, we find some similarities, but also puzzling differences. A major population of ~28 nt long piRNAs is expressed at high levels during *Rhodnius* embryogenesis and comprises sequences of 46 transposon families. Some examples are the *Ty3 retrotransposon*, *RTE-X*, *Helitron*, *Maverick*, *I*, *Penelope* and the abundant class of *Mariner* transposons (Filée et al., 2015). We have referred to all these transposons as resident TEs, but it should be noted that they are frequently involved in horizontal transfer events. For these elements, we find primary piRNAs with the typical 1U bias and secondary piRNAs with Adenine at 10th position (10A) for the sense piRNAs. Also, consistent with an active ping-pong amplification mechanism, sense and antisense piRNA mates overlap by 10 nt. Similar to more basal holometabolous and hemimetabolous insects, but unlike *D. melanogaster*, the ping-pong signal is not restricted to the gonads in *Rhodnius*, but it is especially active in embryonic and in post-embryonic developmental stages. The piRNA complement targeting the HTTs instead displays unique properties. Even though HTT piRNAs are ~28 nt long and display a 1U bias, the ping-pong mechanism is ambiguous. The 10 nt overlap is modest or confused among other signals. Instead, the most abundant *SPIN* and *hAT* piRNA mates display a ~20 nt overlap at their 5′ends. Yet, the 10th position of the sense piRNAs is an Adenine as observed for canonical ping-pong piRNA pairs. These observations suggest that the biogenesis of HTT piRNAs in *Rhodnius* differs from the more canonical mechanism that drives resident TE piRNA maturation and that was described in detail in the fruit fly *D. melanogaster*. The lack of ping-pong signature for the HTTs might reside at least in part in the genomic sources of their piRNAs. In this study, we show that piRNA clusters in *Rhodnius* are mostly of the uni-strand type, but unlike the *Drosophila flam* locus (Brennecke et al., 2007), their TEs are not polarized. For this reason, *Rhodnius* clusters can produce both sense and antisense piRNAs, even though the transcription occurs from one genomic strand. We find that more than 50% of the unique piRNAs targeting resident TEs originate from the piRNA clusters, while these *loci* account for less than 15% of the HTT piRNAs. This observation is consistent with the low number of HTT copies inserted into the clusters. These sequences therefore, might not produce sufficient levels of antisense transcripts to robustly activate the ping-pong mechanism. The *ET* element provides an extreme case, whereby all the cluster copies generate sense piRNAs, thus preventing the production of secondary piRNAs. How the *hAT* and *SPIN* piRNA mates overlapping by ~20 nt are generated and what factors are involved in the mechanism remains to be elucidated. Interestingly, our results reveal that *Rhodnius* expresses siRNAs for resident TEs, but not for the HTTs. Hence, primary piRNAs produced from HTT copies or fragments scattered in the genome, rather than siRNAs, might provide the first line of defense against newly invading transposons in this insect species.

TE siRNA are expressed from piRNA clusters and TE copies dispersed in the genome during oogenesis and to a lesser extent during embryonic and postembryonic stages. RNAi might

contribute to reducing transposon transcripts during oogenesis, although it is unable to completely silence these elements (Coelho et al., 2021). It was recently shown that maternally provided siRNAs loaded in the developing eggs promote piRNA cluster activation in the *Drosophila* embryo (Luo et al., 2023). Unlike *Drosophila*, *Rhodnius* does not produce abundant piRNAs during oogenesis. Thus in *Rhodnius* and other more basal insects, the siRNA complement might be especially critical for jumpstarting piRNA production in early embryonic stages. Transposon downregulation is subsequently taken over by the ~28 nt piRNA pool during embryogenesis. Transposon transcripts maternally deposited in the developing oocytes might feed the ping-pong amplification loop at this stage together with cluster-derived antisense piRNAs. piRNA biogenesis seems to result in the consumption of the cluster-derived piRNA precursors and the downregulation of TEs. In post-embryonic stages instead both siRNAs and piRNAs are reduced, while TE and piRNA cluster transcripts appear to accumulate, thus pointing to a minor sensitivity of the 1st instar nymphs to transposon expression. In support of these conclusions, the levels of piRNAs and siRNAs seem to inversely correlate with those of TEs and piRNA cluster transcripts in all the stages analyzed (Figure 6F).

Rhodnius harbors four *PIWI* genes and the knockdown of *Rp-piwi2*, *Rp-piwi3* and *Rp-ago3* by parental RNAi results in partial or complete female adult sterility (Lu et al., 2011; Brito et al., 2018). Our assays show that these *Rp-PIWI* genes are expressed in embryos and nymphs with *Rp-piwi2* being dramatically upregulated in embryos coinciding with peak levels of ~28 nt piRNAs. Thus, *Rp-piwi2* likely exerts a crucial role in piRNA biogenesis or function. Since Ago3 was shown to coordinate the ping-pong cycle together with Aub in *Drosophila* (Brennecke et al., 2007; Gunawardane et al., 2007), it is tempting to speculate that the protein products of the only *ago3* ortholog in *Rhodnius* (i.e., *Rp-ago3*) and *Rp-piwi2* genes might regulate a similar mechanism in *Rhodnius* embryos. However, *Rp-ago3* might actually act in concert with *Rp-piwi3* in this mechanism. The observation that *Rp-piwi3* expression levels are low in oogenesis and almost undetectable in nymphs, where the ~28 nt piRNAs are barely produced, seem to lend support to this hypothesis. The cell lines that were recently developed from *Rhodnius* embryos will likely provide a valuable tool to dissect the function of the different *Rp-PIWI* genes in piRNA biogenesis and transposon silencing as well as shed light on the transcriptional regulation of the piRNA clusters (Penrice-Randal et al., 2022).

Conclusion

Horizontal transposon transfer has been well characterized in Drosophilids, where numerous instances of P-element transfer from *Drosophila willinstoni* and *Drosophila simulans* to *D. melanogaster* were described (Kidwell, 1983; Anxolabéhère et al., 1988). Fruit flies therefore provided the opportunity to dissect the response of the piRNA pathway to P-element invasion (Asif-Laidin et al., 2023). To our knowledge however, this is the first study to link piRNAs to HTTs exchanged between vertebrates and an hematophagous insect of medical interest. Studies in *Rhodnius* will therefore help shed light on the evolution of the piRNA pathway and on the initial steps of the arms race between invading TEs and small RNA-based defense systems.

Methods

Ethic statement and insect handling

All the experimental protocols involving animals were carried on in accordance with the guidelines of the Committee for Evaluation of Animal Use for Research (Universidade Federal do Rio de Janeiro, CAUAP-UFRJ) and the NIH Guide for the Care and Use of Laboratory Animals (ISBN 0–309–05377–3). Protocols were approved by CAUAP-UFRJ under registry #IBQM155/13. Specialized technicians at the animal facility (Instituto de Bioquímica Médica Leopoldo de Meis, UFRJ) handled the rabbit husbandry under strict guidelines and the supervision of veterinarians.

Insects were maintained at controlled temperature (28°C) and relative humidity (70%–80%) and fed with rabbit blood at regular intervals to promote ecdysis and oogenesis. After the first blood feeding, all adult insects were fed every 21 days. Dissection of the adult females, where necessary, was carried on 7 days after the first or second blood meal. All animal care and experimental protocols were performed according to the ethics guidelines.

Total RNA extraction and small RNA purification

Total RNA for small RNA library preparation was extracted from 30 embryos and 20 1st-instar nymphs for each biological replicate. Embryos were collected over a 48 h period spanning the initial stages of embryogenesis up to the formation of head and thoracic segments (Berni et al., 2014). First-instar nymphs were collected 5 days after hatching and before the first blood feeding regimen. Two biological replicates were produced for each developmental stage. Ovaries were dissected in ice-cold 1X PBS and immediately stored on ice. Previtellogenic tissues and mature eggs were teased apart under light microscopy and subjected to total RNA extraction using Trizol Reagent (Invitrogen) as per manufacturer's instructions. For the production of small RNA libraries, 20 µg of total RNA was separated on polyacrylamide gel containing 15 M Urea (Pane et al., 2011). A gel slice corresponding to 18 to 30 nucleotide RNAs was manually retrieved from the gel and the RNAs were eluted in 3 M NaCl overnight. Finally, RNA was precipitated using 0.7 volumes of Isopropanol and 1 ul Glycogen and resuspended in RNAse-free water. Small RNA library preparation and sequencing were carried out at the Max Planck Institute facility in Freiburg (Germany) with Truseq Small RNA library preparation kit as per manufacturer's protocol (Illumina). Total RNA extracted from 1st instar nymphs was also used to produce and sequence RNA-Seq libraries (Macrogen, Korea). RNA-Seq datasets corresponding to four embryonic stages of *Rhodnius* development were produced by others and are available at NCBI-SRA (Pascual and Rivera-Pomar, 2022) (SRR14606474, SRR14606475 and SRR14606473).

Bioinformatic analysis

Small RNA-Seq libraries were subjected to adaptor removal and trimming using TrimGalore! (Babraham Bioinformatics - Trim Galore, 2024). Reads with length lower than 18 nt were filtered out. Trimmed reads were mapped with Bowtie v1.2 (Langmead et al., 2009) to *Rhodnius prolixus* reference genome available at VectorBase (Giraldo-Calderón et al., 2015) allowing up to 3 mismatches and no more than 50 mappings per read (-v 3 -m 50 -a--best--strata). Qualities were assessed with FastQC software (Babraham Bioinformatics - FastQC A Quality Control tool for High Throughput Sequence Data, 2024), genomic coverages were compared with deepTools (Ramírez et al., 2016) and final quality reports were generated using multiQC (Ewels et al., 2016). Library characterization was performed using featureCounts from the subread package (Liao et al., 2014), where counts to each annotated feature were normalized by number of mappings and overlapping features (-O -M--fraction). Repeats and TEs sequences were *de novo* identified using RepeatModeler v2.0.1 (Flynn et al., 2020)and genomic regions obtained with RepeatMasker v4.1.2 (RepeatMasker Home Page, 2024). Sequences of the HTTs have been previously published (Gilbert et al., 2010). Reads overlapping with TEs, with length distribution of 24–32 nucleotides and not overlapping with miRNAs, rRNAs, snRNAs, simple repeats or low complexity regions were characterized as piRNAs. Sense and antisense piRNAs were separated by overlapping piRNA mappings with TEs annotation using bedtools intersect and forcing strandness (-s and -S). Fasta sequences were extracted using samtools (Li et al., 2009) and sequence logos constructed using ggseqlogo (Wagih, 2017). For ping-pong signal analysis, each sense piRNA was used to search for 5′ to 5′ overlapping antisense piRNAs and the size of the overlap counted for each match. Reads mapped to multiple places in the genome were apportioned. Phasing analysis was done as previously described (Han et al., 2015). For piRNA cluster identification, the chromosome-length genome assembly of *Rhodnius* (https://www.dnazoo.org/assemblies/Rhodnius_prolixus) was used and all the steps described previously were applied to this version as well. First, annotations of a sliding window with 5 kb in size and steps of 1 kb were generated using the makewindow tool from bedtools v2.31 (Quinlan, 2014). Then, bedtools coverage was used to access the uniquely mapped piRNA coverage in each window and only windows with a density greater than 5 piRNAs/kb covering at least 12% of the window were retained. Finally, overlapping windows were merged and merged windows with a distance less than 20 kb from each other were combined to produce the final piRNA clusters. RNA-seq data were pre-processed and aligned using snakePipes (Bhardwaj et al., 2019). Genes and transposable element read counts were produced using featureCounts allowing fraction counts for overlapping features. Final expression was calculated as Reads Per Kilobase per Million (RPKM).

Quantitative RT-PCR assays

Quantitative RT-PCR assays were carried out with three biological replicates. 1 ug of total RNA extracted with Trizol (Invitrogen) was submitted to DNAse treatment with Turbo DNAse free kit (Ambion) and cDNA synthesis using the MultiScribe Reverse Transcriptase (Thermo Fisher Scientific) as per manufacturer's instructions. The resulting cDNAs were used for qPCR assays with the set of oligonucleotides previously described (Brito et al., 2018). Roughly 50 ng of cDNA for each sample was mixed with oligonucleotides specific to target genes and SYBR green reagent (Life Technologies). qRT-PCR was carried on QuantStudio 7 Flex (ThermoFisher). Fold change differences were plotted as $2^{-\Delta Ct}$. Statistical analyses were performed using one-way ANOVA followed by Turkey HSD *post hoc* test for pairwise comparisons.

Data availability statement

Original datasets are available publicly at the Sequence Read Archive (SRA) database and are all part of the Bioproject PRJNA724683.

Ethics statement

The manuscript presents research on animals that do not require ethical approval for their study.

Author contributions

TB: Data curation, Formal Analysis, Investigation, Methodology, Validation, Visualization, Writing–original draft, Writing–review and editing. MA: Data curation, Investigation, Methodology, Validation, Writing–original draft, Writing–review and editing. NA: Investigation, Writing–review and editing. IA: Investigation, Methodology, Writing–original draft. LA: Investigation, Writing–original draft. NI: Data curation, Funding acquisition, Resources, Writing–original draft, Writing–review and editing. AP: Conceptualization, Data curation, Formal Analysis, Funding acquisition, Investigation, Methodology, Project administration, Resources, Supervision, Validation, Visualization, Writing–original draft, Writing–review and editing.

Funding

The author(s) declare that financial support was received for the research, authorship, and/or publication of this article. This work was supported by the National Counsel of Technological and Scientific Development (CNPq) (428100/2018-0) (AP), the Research Support Foundation of the State of Rio de Janeiro (FAPERJ) E-26/210.912/2019 (AP); E-26/010.002720/2019 (AP); E-26/010.001877/2015 (AP); E-26/201.703/2021 (TB), Wellcome Trust grant 207486Z17Z (AP/ABC), CAPES and INCT/Enem fundings (AP, TB, MA, IA). NA is supported by the Max Planck Society and IMPRS program. NI is supported by the Max Planck Society; DFG:CRC992, Project B06; Behrens-Weise Stiftung; CIBSS - EXC 2189. Also, this project has received funding from the European Research Council (ERC) under the European Union's Horizon 2020 research and innovation programme (grant agreement No.819941) ERC CoG, EpiRIME. The funders had no

role in study design, data collection and analysis, decision to publish, or preparation of the manuscript.

Acknowledgments

We would like to thank Bernardo Carvalho, Pedro Lagerblad de Oliveira, Ana Cristina Bahia Nascimento, Marcos Farina de Souza e Marcia Cury El-Cheikh for their constant support. We are grateful to Eric Aguiar and members of the Functional Genomics Laboratory for helpful suggestions and critical reading of the manuscript. We thank Kelli Cristina Melquiades Mendes, Daniela Sodré Leal and Graciela Venturi for the invaluable technical support.

Conflict of interest

The authors declare that the research was conducted in the absence of any commercial or financial relationships that could be construed as a potential conflict of interest.

Publisher's note

All claims expressed in this article are solely those of the authors and do not necessarily represent those of their affiliated organizations, or those of the publisher, the editors and the reviewers. Any product that may be evaluated in this article, or claim that may be made by its manufacturer, is not guaranteed or endorsed by the publisher.

Supplementary material

The Supplementary Material for this article can be found online at: https://www.frontiersin.org/articles/10.3389/fcell.2024.1481881/full#supplementary-material

SUPPLEMENTARY FIGURE S1
Abundance of transposon families in the top 10 piRNA clusters. *X*-axis displays the number of elements found for each transposon family (*Y*-axis) in each of the top 10 piRNA clusters. Since the "Unknown" elements are the most abundant ones, they are shown separately at the bottom.

SUPPLEMENTARY FIGURE S2
Partially sequenced region in RPCL2. Positive (blue) and negative (red) read coverage along the piRNA cluster RPCL2 (top). At first inspection, RPCL2 seems like a bidirectional cluster. However, when looking at the exact region where the expression shifts (bottom), a partially sequenced region is notable and might represent an assembly error.

SUPPLEMENTARY TABLE S1
General mapping statistics.

SUPPLEMENTARY TABLE S2
piRNA identification and pairing information.

References

Adaptation to P Element Transposon Invasi, on in Drosophila melanogaster. Khurana, J. S., Wang, J., Xu, J., Koppetsch, B. S., Thomson, T. C., Nowosielska, A., et al. (2011). Adaptation to P element transposon invasion in Drosophila melanogaster. *Cell* 147, 1551–1563. doi:10.1016/j.cell.2011.11.042

Andersen, P. R., Tirian, L., Vunjak, M., and Brennecke, J. (2017). A heterochromatin-dependent transcription machinery drives piRNA expression. *Nature* 549, 54–59. doi:10.1038/nature23482

Anxolabéhère, D., Kidwell, M. G., and Periquet, G. (1988). Molecular characteristics of diverse populations are consistent with the hypothesis of a recent invasion of Drosophila melanogaster by mobile P elements. *Mol. Biol. Evol.* 5, 252–269. doi:10.1093/oxfordjournals.molbev.a040491

Aravin, A. A., Hannon, G. J., and Brennecke, J. (2007). The Piwi-piRNA pathway provides an adaptive defense in the transposon arms race. *Science* 318, 761–764. doi:10.1126/science.1146484

Aravin, A. A., Naumova, N. M., Tulin, A. V., Vagin, V. V., Rozovsky, Y. M., and Gvozdev, V. A. (2001). Double-stranded RNA-mediated silencing of genomic tandem repeats and transposable elements in the *D. melanogaster* germline. *Curr. Biol.* 11, 1017–1027. doi:10.1016/s0960-9822(01)00299-8

Asif-Laidin, A., Casier, K., Ziriat, Z., Boivin, A., Viodé, E., Delmarre, V., et al. (2023). Modeling early germline immunization after horizontal transfer of transposable elements reveals internal piRNA cluster heterogeneity. *BMC Biol.* 21, 117. doi:10.1186/s12915-023-01616-z

Babraham Bioinformatics - FastQC A Quality Control tool for High Throughput Sequence Data (2024). Available at: https://www.bioinformatics.babraham.ac.uk/projects/fastqc/ (Accessed October 1, 2023).

Babraham Bioinformatics - Trim Galore (2024). Available at: https://www.bioinformatics.babraham.ac.uk/projects/trim_galore/ (Accessed October 1, 2023).

Berni, M., Fontenele, M. R., Tobias-Santos, V., Caceres-Rodrigues, A., Mury, F. B., Vionette-do-Amaral, R., et al. (2014). Toll signals regulate dorsal-ventral patterning and anterior-posterior placement of the embryo in the hemipteran Rhodnius prolixus. *Evodevo* 5, 38. doi:10.1186/2041-9139-5-38

Bernstein, E., Caudy, A. A., Hammond, S. M., and Hannon, G. J. (2001). Role for a bidentate ribonuclease in the initiation step of RNA interference. *Nature* 409, 363–366. doi:10.1038/35053110

Bhardwaj, V., Heyne, S., Sikora, K., Rabbani, L., Rauer, M., Kilpert, F., et al. (2019). snakePipes: facilitating flexible, scalable and integrative epigenomic analysis. *Bioinf.* 35 (22), 4757–4759. doi:10.1093/bioinformatics/btz436

Brennecke, J., Aravin, A. A., Stark, A., Dus, M., Kellis, M., Sachidanandam, R., et al. (2007). Discrete small RNA-generating loci as master regulators of transposon activity in Drosophila. *Cell* 128, 1089–1103. doi:10.1016/j.cell.2007.01.043

Brennecke, J., Malone, C. D., Aravin, A. A., Sachidanandam, R., Stark, A., and Hannon, G. J. (2008). An epigenetic role for maternally inherited piRNAs in transposon silencing. *Science* 322, 1387–1392. doi:10.1126/science.1165171

Brito, T., Julio, A., Berni, M., de Castro Poncio, L., Bernardes, E. S., Araujo, H., et al. (2018). Transcriptomic and functional analyses of the piRNA pathway in the Chagas disease vector Rhodnius prolixus. *PLoS Negl. Trop. Dis.* 12, e0006760. doi:10.1371/journal.pntd.0006760

Brito, T. F. de, Coelho, V. L., Cardoso, M. A., Brito, I. A. de A., Berni, M. A., Zenk, F. L., et al. (2021). Transovarial transmission of a core virome in the Chagas disease vector Rhodnius prolixus. *PLoS Pathog.* 17, e1009780. doi:10.1371/journal.ppat.1009780

Buxton, P. A. (1930). The biology of a blood-sucking bug, rhodnius prolixus. *Trans. R. Entomological Soc. Lond.* 78, 227–256. doi:10.1111/j.1365-2311.1930.tb00385.x

Carvalho, T. L., Cordeiro, J., Vizentin-Bugoni, J., Fonseca, P. M., Loreto, E. L. S., and Robe, L. J. (2023). Horizontal transposon transfer and their ecological drivers: the case of flower-breeding Drosophila. *Genome Biol. Evol.* 15, evad068. doi:10.1093/gbe/evad068

Chary, S., and Hayashi, R. (2023). The absence of core piRNA biogenesis factors does not impact efficient transposon silencing in Drosophila. *PLoS Biol.* 21, e3002099. doi:10.1371/journal.pbio.3002099

Coelho, V. L., de Brito, T. F., de Abreu Brito, I. A., Cardoso, M. A., Berni, M. A., Araujo, H. M. M., et al. (2021). Analysis of ovarian transcriptomes reveals thousands of novel genes in the insect vector Rhodnius prolixus. *Sci. Rep.* 11, 1918. doi:10.1038/s41598-021-81387-1

Cox, D. N., Chao, A., and Lin, H. (2000). Piwi encodes a nucleoplasmic factor whose activity modulates the number and division rate of germline stem cells. *Development* 127, 503–514. doi:10.1242/dev.127.3.503

Czech, B., Malone, C. D., Zhou, R., Stark, A., Schlingeheyde, C., Dus, M., et al. (2008). An endogenous small interfering RNA pathway in Drosophila. *Nature* 453, 798–802. doi:10.1038/nature07007

Czech, B., Munafò, M., Ciabrelli, F., Eastwood, E. L., Fabry, M. H., Kneuss, E., et al. (2018). piRNA-Guided genome defense: from biogenesis to silencing. *Annu. Rev. Genet.* 52, 131–157. doi:10.1146/annurev-genet-120417-031441

Daniels, S. B., Peterson, K. R., Strausbaugh, L. D., Kidwell, M. G., and Chovnick, A. (1990). Evidence for horizontal transmission of the P transposable element between Drosophila species. *Genetics* 124, 339–355. doi:10.1093/genetics/124.2.339

Dowling, D., Pauli, T., Donath, A., Meusemann, K., Podsiadlowski, L., Petersen, M., et al. (2016). Phylogenetic origin and diversification of RNAi pathway genes in insects. *Genome Biol. Evol.* 8, 3784–3793. doi:10.1093/gbe/evw281

Ewels, P., Magnusson, M., Lundin, S., and Käller, M. (2016). MultiQC: summarize analysis results for multiple tools and samples in a single report. *Bioinformatics* 32, 3047–3048. doi:10.1093/bioinformatics/btw354

Filée, J., Rouault, J.-D., Harry, M., and Hua-Van, A. (2015). Mariner transposons are sailing in the genome of the blood-sucking bug Rhodnius prolixus. *BMC Genomics* 16, 1061. doi:10.1186/s12864-015-2060-9

Flynn, J. M., Hubley, R., Goubert, C., Rosen, J., Clark, A. G., Feschotte, C., et al. (2020). RepeatModeler2 for automated genomic discovery of transposable element families. *Proc. Natl. Acad. Sci. U. S. A.* 117, 9451–9457. doi:10.1073/pnas.1921046117

Gainetdinov, I., Colpan, C., Arif, A., Cecchini, K., and Zamore, P. D. (2018). A single mechanism of biogenesis, initiated and directed by PIWI proteins, explains piRNA production in most animals. *Mol. Cell* 71, 775–790. doi:10.1016/j.molcel.2018.08.007

Gao, D., Chu, Y., Xia, H., Xu, C., Heyduk, K., Abernathy, B., et al. (2017). Horizontal transfer of non-LTR retrotransposons from arthropods to flowering plants. *Mol. Biol. Evol.* 35, 354–364. doi:10.1093/molbev/msx275

Gilbert, C., Schaack, S., Pace, J. K. I. I., Brindley, P. J., and Feschotte, C. (2010). A role for host–parasite interactions in the horizontal transfer of transposons across phyla. *Nature* 464, 1347–1350. doi:10.1038/nature08939

Giraldo-Calderón, G. I., Emrich, S. J., MacCallum, R. M., Maslen, G., Dialynas, E., Topalis, P., et al. (2015). VectorBase: an updated bioinformatics resource for invertebrate vectors and other organisms related with human diseases. *Nucleic Acids Res.* 43, D707–D713. doi:10.1093/nar/gku1117

Gunawardane, L. S., Saito, K., Nishida, K. M., Miyoshi, K., Kawamura, Y., Nagami, T., et al. (2007). A slicer-mediated mechanism for repeat-associated siRNA 5′ end formation in Drosophila. *Science* 315, 1587–1590. doi:10.1126/science.1140494

Han, B. W., Wang, W., Li, C., Weng, Z., and Zamore, P. D. (2015). Noncoding RNA. piRNA-guided transposon cleavage initiates Zucchini-dependent, phased piRNA production. *Science* 348, 817–821. doi:10.1126/science.aaa1264

Hubley, R., Finn, R. D., Clements, J., Eddy, S. R., Jones, T. A., Bao, W., et al. (2016). The Dfam database of repetitive DNA families. *Nucleic Acids Res.* 44, D81–D89. doi:10.1093/nar/gkv1272

Kawamura, Y., Saito, K., Kin, T., Ono, Y., Asai, K., Sunohara, T., et al. (2008). Drosophila endogenous small RNAs bind to Argonaute 2 in somatic cells. *Nature* 453, 793–797. doi:10.1038/nature06938

Kidwell, M. G. (1983). Hybrid dysgenesis in DROSOPHILA MELANOGASTER: factors affecting chromosomal contamination in the P-M system. *Genetics* 104, 317–341. doi:10.1093/genetics/104.2.317

Kidwell, M. G., Kidwell, J. F., and Sved, J. A. (1977). Hybrid dysgenesis in DROSOPHILA melanogaster: a syndrome of aberrant traits including mutation, sterility and male recombination. *Genetics* 86, 813–833. doi:10.1093/genetics/86.4.813

Kidwell, M. G., Kimura, K., and Black, D. M. (1988). Evolution of hybrid dysgenesis potential following P element contamination in Drosophila melanogaster. *Genetics* 119, 815–828. doi:10.1093/genetics/119.4.815

Klattenhoff, C., Xi, H., Li, C., Lee, S., Xu, J., Khurana, J. S., et al. (2009). The Drosophila HP1 homolog Rhino is required for transposon silencing and piRNA production by dual-strand clusters. *Cell* 138, 1137–1149. doi:10.1016/j.cell.2009.07.014

Kofler, R., Hill, T., Nolte, V., Betancourt, A. J., and Schlötterer, C. (2015). The recent invasion of natural Drosophila simulans populations by the P-element. *Proc. Natl. Acad. Sci. U. S. A.* 112, 6659–6663. doi:10.1073/pnas.1500758112

Lander, E. S., Linton, L. M., Birren, B., Nusbaum, C., Zody, M. C., Baldwin, J., et al. (2001). Initial sequencing and analysis of the human genome. *Nature* 409, 860–921. doi:10.1038/35057062

Langmead, B., Trapnell, C., Pop, M., and Salzberg, S. L. (2009). Ultrafast and memory-efficient alignment of short DNA sequences to the human genome. *Genome Biol.* 10, R25. doi:10.1186/gb-2009-10-3-r25

Lee, Y. S., Nakahara, K., Pham, J. W., Kim, K., He, Z., Sontheimer, E. J., et al. (2004). Distinct roles for Drosophila Dicer-1 and Dicer-2 in the siRNA/miRNA silencing pathways. *Cell* 117, 69–81. doi:10.1016/s0092-8674(04)00261-2

Le Thomas, A., Rogers, A. K., Webster, A., Marinov, G. K., Liao, S. E., Perkins, E. M., et al. (2013). Piwi induces piRNA-guided transcriptional silencing and establishment of a repressive chromatin state. *Genes Dev.* 27, 390–399. doi:10.1101/gad.209841.112

Li, H., Handsaker, B., Wysoker, A., Fennell, T., Ruan, J., Homer, N., et al. (2009). The sequence alignment/map format and SAMtools. *Bioinformatics* 25, 2078–2079. doi:10.1093/bioinformatics/btp352

Li, Y., Liu, Z., Liu, C., Shi, Z., Pang, L., Chen, C., et al. (2022). HGT is widespread in insects and contributes to male courtship in lepidopterans. *Cell* 185, 2975–2987.e10. doi:10.1016/j.cell.2022.06.014

Liao, Y., Smyth, G. K., and Shi, W. (2014). featureCounts: an efficient general purpose program for assigning sequence reads to genomic features. *Bioinformatics* 30, 923–930. doi:10.1093/bioinformatics/btt656

Liu, C., Li, Y., Chen, Y., Chen, X.-X., Huang, J., Rokas, A., et al. (2023). How has horizontal gene transfer shaped the evolution of insect genomes? *Environ. Microbiol.* 25, 642–645. doi:10.1111/1462-2920.16311

Llonga, N., Ylla, G., Bau, J., Belles, X., and Piulachs, M.-D. (2018). Diversity of piRNA expression patterns during the ontogeny of the German cockroach. *J. Exp. Zool. B Mol. Dev. Evol.* 330, 288–295. doi:10.1002/jez.b.22815

Lu, H.-L., Tanguy, S., Rispe, C., Gauthier, J.-P., Walsh, T., Gordon, K., et al. (2011). Expansion of genes encoding piRNA-associated argonaute proteins in the pea aphid: diversification of expression profiles in different plastic morphs. *PLoS One* 6, e28051. doi:10.1371/journal.pone.0028051

Luo, Y., He, P., Kanrar, N., Fejes Toth, K., and Aravin, A. A. (2023). Maternally inherited siRNAs initiate piRNA cluster formation. *Mol. Cell* 83, 3835–3851.e7. doi:10.1016/j.molcel.2023.09.033

Malone, C. D., Brennecke, J., Dus, M., Stark, A., McCombie, W. R., Sachidanandam, R., et al. (2009). Specialized piRNA pathways act in germline and somatic tissues of the Drosophila ovary. *Cell* 137, 522–535. doi:10.1016/j.cell.2009.03.040

Mesquita, R. D., Vionette-Amaral, R. J., Lowenberger, C., Rivera-Pomar, R., Monteiro, F. A., Minx, P., et al. (2015). Genome of Rhodnius prolixus, an insect vector of Chagas disease, reveals unique adaptations to hematophagy and parasite infection. *Proc. Natl. Acad. Sci. U. S. A.* 112, 14936–14941. doi:10.1073/pnas.1506226112

Mohn, F., Sienski, G., Handler, D., and Brennecke, J. (2014). The rhino-deadlock-cutoff complex licenses noncanonical transcription of dual-strand piRNA clusters in Drosophila. *Cell* 157, 1364–1379. doi:10.1016/j.cell.2014.04.031

Montiel, E. E., Panzera, F., Palomeque, T., Lorite, P., and Pita, S. (2021). Satellitome analysis of Rhodnius prolixus, one of the main Chagas disease vector species. *Int. J. Mol. Sci.* 22, 6052. doi:10.3390/ijms22116052

Ninova, M., Griffiths-Jones, S., and Ronshaugen, M. (2017). Abundant expression of somatic transposon-derived piRNAs throughout Tribolium castaneum embryogenesis. *Genome Biol.* 18, 184. doi:10.1186/s13059-017-1304-1

Pane, A., Jiang, P., Zhao, D. Y., Singh, M., and Schüpbach, T. (2011). The Cutoff protein regulates piRNA cluster expression and piRNA production in the Drosophila germline. *EMBO J.* 30, 4601–4615. doi:10.1038/emboj.2011.334

Pascual, A., and Rivera-Pomar, R. (2022). Dynamics of maternal gene expression in Rhodnius prolixus. *Sci. Rep.* 12, 6538. doi:10.1038/s41598-022-09874-7

Peccoud, J., Loiseau, V., Cordaux, R., and Gilbert, C. (2017). Massive horizontal transfer of transposable elements in insects. *Proc. Natl. Acad. Sci. U. S. A.* 114, 4721–4726. doi:10.1073/pnas.1621178114

Pélisson, A., Song, S. U., Prud'homme, N., Smith, P. A., Bucheton, A., and Corces, V. G. (1994). Gypsy transposition correlates with the production of a retroviral envelope-like protein under the tissue-specific control of the Drosophila flamenco gene. *EMBO J.* 13, 4401–4411. doi:10.1002/j.1460-2075.1994.tb06760.x

Penrice-Randal, R., Hartley, C., Beliavskaia, A., Dong, X., Brandner-Garrod, L., Whitten, M., et al. (2022). New cell lines derived from laboratory colony Triatoma infestans and Rhodnius prolixus, vectors of trypanosoma cruzi, do not harbour Triatoma virus. *Insects* 13, 906. doi:10.3390/insects13100906

Quinlan, A. R. (2014). BEDTools: the Swiss-army tool for genome feature analysis. *Curr. Protoc. Bioinforma.* 47 (11.12), 1–34. doi:10.1002/0471250953.bi1112s47

Ramírez, F., Ryan, D. P., Grüning, B., Bhardwaj, V., Kilpert, F., Richter, A. S., et al. (2016). deepTools2: a next generation web server for deep-sequencing data analysis. *Nucleic Acids Res.* 44, W160–W165. doi:10.1093/nar/gkw257

RepeatMasker Home Page (2024). RepeatMasker. Available at: http://www.repeatmasker.org (Accessed December 22, 2023).

Robinson, J. T., Thorvaldsdóttir, H., Winckler, W., Guttman, M., Lander, E. S., Getz, G., et al. (2011). Integrative genomics viewer. *Nat. Biotechnol.* 29, 24–26. doi:10.1038/nbt.1754

Rosenkranz, D., Rudloff, S., Bastuck, K., Ketting, R. F., and Zischler, H. (2015). Tupaia small RNAs provide insights into function and evolution of RNAi-based transposon defense in mammals. *RNA* 21, 911–922. doi:10.1261/rna.048603.114

Saito, K., Ishizu, H., Komai, M., Kotani, H., Kawamura, Y., Nishida, K. M., et al. (2010). Roles for the Yb body components Armitage and Yb in primary piRNA biogenesis in Drosophila. *Genes Dev.* 24, 2493–2498. doi:10.1101/gad.1989510

SanMiguel, P., Tikhonov, A., Jin, Y. K., Motchoulskaia, N., Zakharov, D., Melake-Berhan, A., et al. (1996). Nested retrotransposons in the intergenic regions of the maize genome. *Science* 274, 765–768. doi:10.1126/science.274.5288.765

Santos, D., Feng, M., Kolliopoulou, A., Taning, C. N. T., Sun, J., and Swevers, L. (2023). What are the functional roles of piwi proteins and piRNAs in insects? *Insects* 14, 187. doi:10.3390/insects14020187

Sienski, G., Dönertas, D., and Brennecke, J. (2012). Transcriptional silencing of transposons by Piwi and maelstrom and its impact on chromatin state and gene expression. *Cell* 151, 964–980. doi:10.1016/j.cell.2012.10.040

Wagih, O. (2017). ggseqlogo: a versatile R package for drawing sequence logos. *Bioinformatics* 33, 3645–3647. doi:10.1093/bioinformatics/btx469

Wang, W., Ashby, R., Ying, H., Maleszka, R., and Forêt, S. (2017). Contrasting sex-and caste-dependent piRNA profiles in the transposon depleted haplodiploid honeybee Apis mellifera. *Genome Biol. Evol.* 9, 1341–1356. doi:10.1093/gbe/evx087

Xia, J., Guo, Z., Yang, Z., Han, H., Wang, S., Xu, H., et al. (2021). Whitefly hijacks a plant detoxification gene that neutralizes plant toxins. *Cell* 184, 3588–1705. doi:10.1016/j.cell.2021.06.010

Yin, H., and Lin, H. (2007). An epigenetic activation role of Piwi and a Piwi-associated piRNA in Drosophila melanogaster. *Nature* 450, 304–308. doi:10.1038/nature06263

Zanni, V., Eymery, A., Coiffet, M., Zytnicki, M., Luyten, I., Quesneville, H., et al. (2013). Distribution, evolution, and diversity of retrotransposons at the flamenco locus reflect the regulatory properties of piRNA clusters. *Proc. Natl. Acad. Sci. U. S. A.* 110, 19842–19847. doi:10.1073/pnas.1313677110

Zhang, H.-H., Peccoud, J., Xu, M.-R.-X., Zhang, X.-G., and Gilbert, C. (2020). Horizontal transfer and evolution of transposable elements in vertebrates. *Nat. Commun.* 11, 1362. doi:10.1038/s41467-020-15149-4